arXiv:1302.1613v2 [astro-ph.GA] 27 Feb 2013

METALLICITY GRADIENTS THROUGH DISK INSTABILITY: A SIMPLE MODEL FOR THE MILKY WAY'S BOXY BULGE

Inma Martinez-Valpuesta[1] and Ortwin Gerhard[1]
Max-Planck-Institut für Extraterrestrische Physik, Giessenbachstrasse, 85748 Garching, Germany
Draft version March 1, 2013

ABSTRACT

Observations show a clear vertical metallicity gradient in the Galactic bulge, which is often taken as a signature of dissipative processes in the formation of a classical bulge. Various evidence shows, however, that the Milky Way is a barred galaxy with a boxy bulge representing the inner three-dimensional part of the bar. Here we show with a secular evolution N-body model that a boxy bulge formed through bar and buckling instabilities can show vertical metallicity gradients similar to the observed gradient, if the initial axisymmetric disk had a comparable radial metallicity gradient. In this framework the range of metallicities in bulge fields constrains the chemical structure of the Galactic disk at early times, before bar formation. Our secular evolution model was previously shown to reproduce inner Galaxy star counts and we show here that it also has cylindrical rotation. We use it to predict a full mean metallicity map across the Galactic bulge from a simple metallicity model for the initial disk. This map shows a general outward gradient on the sky as well as longitudinal perspective asymmetries. We also briefly comment on interpreting metallicity gradient observations in external boxy bulges.

Subject headings: Galaxy: structure — Galaxy: bulge — Galaxy: abundances — Galaxy: kinematics and dynamics — galaxies: evolution — methods: numerical

1. INTRODUCTION

About half of edge-on disk galaxies contain boxy or peanut-shaped bulges (BPBs, Lütticke et al. 2000). Their photometric and kinematic properties are consistent with predictions from disk galaxy simulations in which a BPB formed through bar and buckling instabilities (Bureau & Freeman 1999; Debattista et al. 2004; Bureau & Athanassoula 2005). The Galactic bulge shows many characteristics of a BPB formed in this way: a boxy shape in projection (Dwek et al. 1995; Skrutskie et al. 2006); a triaxial density distribution (Binney et al. 1997; López-Corredoira et al. 2005) with a dense inner, rounder component (Gonzalez et al. 2012; Gerhard & Martinez-Valpuesta 2012, hereafter GMV12); an X-shaped structure (McWilliam & Zoccali 2010; Nataf et al. 2010; Ness et al. 2012a; Li & Shen 2012); cylindrical rotation (Howard et al. 2009; Shen et al. 2010); and a transition to an outer planar bar (Martinez-Valpuesta & Gerhard 2011, hereafter MVG11), seen in star count observations as 'long bar' (Benjamin et al. 2005; Cabrera-Lavers et al. 2007).

The Galactic bulge is also known to consist of predominantly old stars (Zoccali et al. 2003; Clarkson et al. 2008) with a broad, asymmetric metallicity distribution function (MDF) (Rich 1990; Ibata & Gilmore 1995; Zoccali et al. 2003). The data clearly show a vertical metallicity gradient, such that the more metal-rich part of the MDF thins out towards high latitudes ($b < -4°$, Minniti et al. 1995; Zoccali et al. 2008; Gonzalez et al. 2011). At latitudes lower than Baade's window ($-4° < b < 0°$) no vertical gradient is seen (Rich et al. 2007, 2012). These properties are not obviously reconciled with a disk origin of the bulge. Because bars tend to mix stars from different radii and so wash out preexisting metal-

licity gradients (Friedli et al. 1994), the observed metallicity gradient in the Galactic bulge has long been taken as a signature for a classical bulge in the Milky Way. Indeed, Bekki & Tsujimoto (2011) found that they could not reproduce the observed gradient with a simulated boxy bulge which had evolved from a pure disk with an initial metallicity gradient. In order to obtain the lower mean metallicities at high b, they needed to include an additional metal-poor thick disk in their initial model.

Here we show with the help of a suitable boxy bulge/bar simulation, that contrary to widespread belief boxy bulges can have metallicity gradients similar to those observed in our Galaxy and in other boxy bulges, if they evolve from disks with similarly steep radial metallicity gradients.

2. N-BODY MODEL FOR THE GALACTIC BAR AND BOXY BULGE

The simulation used in this work is that already analyzed in MVG11 and GMV12, with similar characteristics as described in Martinez-Valpuesta et al. (2006). The model evolved from an exponential disk, with $Q = 1.5$, initial radial scale length of $h = 1.29$ kpc and vertical scale height of $h_z = 0.225$ kpc, embedded in a dark matter halo. Following bar and buckling instabilities it developed a prominent boxy bulge which is already relaxed at ~ 1.5 Gyr. As in GMV12 we consider the simulated galaxy at time $T_b \simeq 1.9$ Gyr when the bar has resumed its growth through further angular momentum transfer to the halo, and we vertically symmetrize the particle distribution to optimize the resolution.

We showed previously that this model reproduces different Milky Way star count observations, both near the Galactic plane for the long bar out to $l \sim 27°$ (MVG11), and in the inner boxy bulge for $-10° \leq l \leq 10°$ and $b = \pm 1°$ (GMV12) as well as for $b = -5°$, where the
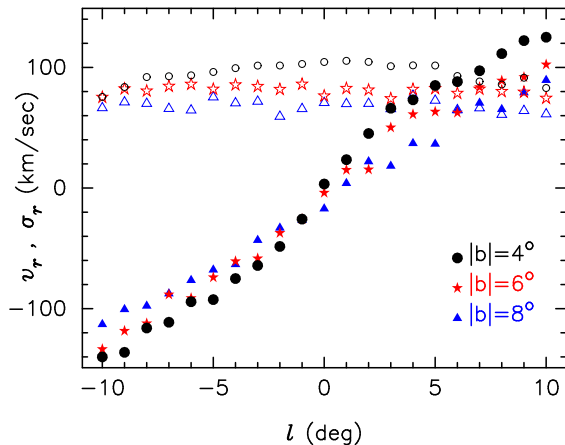
FIG. 1.— Mean radial velocity and velocity dispersion versus longitude for the model's boxy bulge, as seen from the Sun for different latitudes $|b| = 4°, 6°, 8°$. Note how the dispersion decreases with latitude, and that in this projection the rotation is only approximately cylindrical; i.e., the slope of the velocity curve increases slightly towards the plane, as also seen in the Galactic bulge data.

FIG. 2.— Longitudinal and vertical metallicity profiles of the model as seen from the Sun. Left: with l for $|b| = 2°, 4°, 8°$; the gradient along l decreases towards larger distances from the Galactic plane. Right: with $|b|$ for $l = 0°, 5°, 10°$; the vertical gradient decreases with distance from the minor axis.

predictions of the model were subsequently confirmed by Gonzalez et al. (2012). Here we show that the model's boxy bulge at that time also shows approximate cylindrical rotation, with the slope of the mean velocity curve along l increasing slightly towards lower latitudes; see Fig. 1. This is similar to the BRAVA kinematic data (Howard et al. 2009) and the simulation by Shen et al. (2010). The cylindrical rotation in boxy bulges is clearest in edge-on view, as shown in previous simulations (e.g., Combes et al. 1990; Athanassoula & Misiriotis 2002); it is weakened by the nearly end-on orientation of the Milky Way bar and the perspective effects. As in our previous work (MVG11, GMV12), we here take the solar galactocentric distance $D_\odot = 8$ kpc, scale the bar length to 4.5 kpc, and use a bar orientation of $\alpha = 25°$ with respect to the Sun-Galactic center line.

We study the formation of bulge metallicity gradients in the unstable disk – boxy bulge scenario with a simple illustrative model. We assume that the initial exponential disk follows a specified radial metallicity gradient, which we imagine is set up during disk build-up prior to bar formation. We assign to each particle a metallicity depending on its initial radius (e.g., Friedli et al. 1994), according to $[M/H](R) = [M/H]_0 + \alpha_R \times R/\text{kpc}$. After some exploration we choose $[M/H]_0 = 0.6$ and $\alpha_R = -0.4$. Unlike Bekki & Tsujimoto (2011), we do not link these metallicities to the present-day Galactic disk near the Sun, because the buckling instability in the Milky Way must have happened long ago when the outer disk may have been only incompletely assembled.

3. RESULTS

3.1. *Vertical metallicity gradient in the Milky Way bulge*

The bar and buckling instabilities leading to the formation of the boxy bulge strongly change the particle orbits. Thereby the initial disk metallicity distribution is mapped into the bulge accordingly. Fig. 2 shows longitudinal and vertical metallicity profiles for the bulge at T_b. The vertical gradient for $3° < |b| < 7°$ along the minor axis is $\alpha_b = -0.064$ dex/deg, compared to the observed slope in the Milky Way bulge $\alpha_{MW} = -0.075$ dex/deg

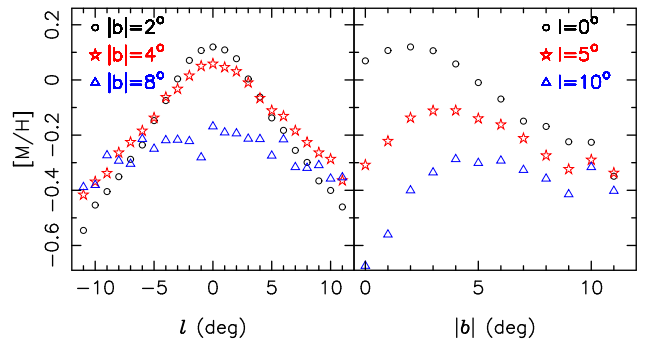from Zoccali et al. (2008) and $\alpha_b = -0.06$ dex/deg from Gonzalez et al. (2011). Near the Galactic plane, $|b| < 3°$, the vertical gradient becomes flatter and even positive. The positive gradient is due to the contamination from foreground/background disk particles. The flat part comes from the mixing during the buckling instability in the inner regions that evolve into the central near-spheroidal component (GMV12), and also from the greater fraction of low-latitude outer bar particles. The absence of a clear vertical gradient near the Galactic plane is consistent with recent results from Rich et al. (2007, 2012). However, their measured mean metallicities for M-giants ([Fe/H]$\simeq -0.2$) are slightly lower in Baade's window than those for K-giants (Zoccali et al. 2008) and for our simple model.

Fig. 3 shows the resulting MDFs in several minor axis fields in the boxy bulge at $T_b = 1.9$ Gyr. Note the clear gradient of mean metallicity with latitude, and that similarly to the observed histograms, it arises mostly from the decreasing fraction of higher metallicity stars away from the Galactic plane. The maximum metallicity in all histograms is $\simeq 0.6$, the central value in the initial disk, and the lowest value is $\simeq -1.2$. 2 Gyr later, at $T_b = 4$ Gyr, the model metallicity gradient is nearly identical, while the mean metallicities in the minor axis fields have slightly decreased, due to the capture of lower-metallicity disk stars by the slowly growing bar. Had we assumed a shallower radial gradient in the initial disk, also the final vertical gradient in the bulge would be smaller.

3.2. *Full metallicity map for the boxy bulge*

So far we have shown that a radial metallicity gradient in the unstable initial disk can survive through the bar and buckling instabilities, and generate, for suitable parameters, a vertical metallicity gradient similar to that observed in the Milky Way bulge. For comparison with upcoming survey results (e.g., VVV, ARGOS, Gaia-ESO), we now provide a full metallicity map, which gives a different view of the predicted metallicities for this scenario. Differently from Fig. 3, we exclude foreground/background disk stars with a distance cut, using only particles with $4 < D < 12$ kpc from the position of the Sun. The assumed initial disk metallicity distribution and simulated galaxy snapshot are as before. Fig. 4 shows the resulting average bulge metallicity map over the area on the sky extended by the Galactic bulge. It
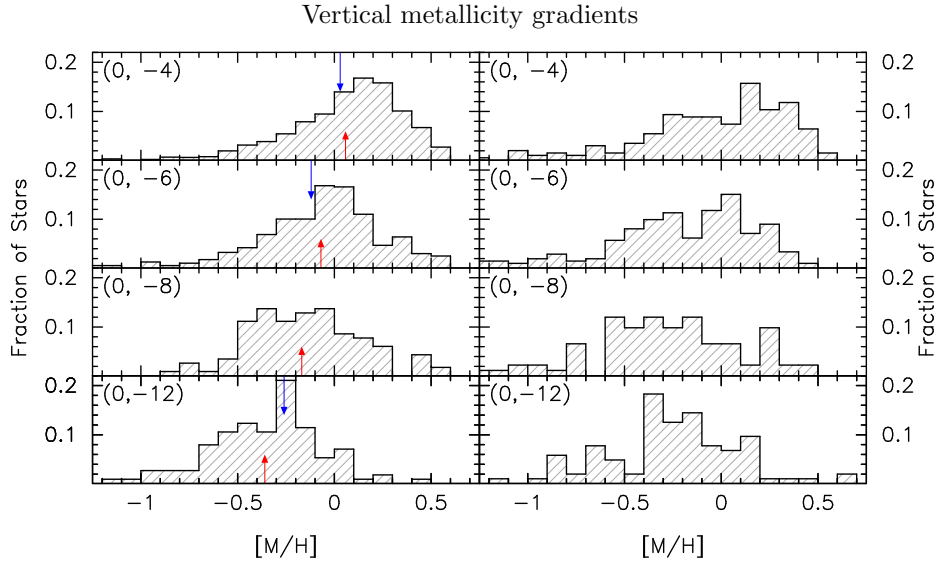
FIG. 3.— Metallicity histograms (MDFs) for model particles in 4 fields along the minor axis of the boxy bulge (*left panels*). The mean value for each MDF is given by the red arrow pointing up from the bottom. The corresponding mean value for the data of Zoccali et al. (2008) is indicated by the blue arrow from the top. The histograms in the *right panels* are based on data from Zoccali et al. (2008) for $b = -4°, -6°, -12°$, and from Johnson et al. (2011) for $b = -8°$.

has several noteworthy properties:

(i) The approximate outline of the boxy bulge can be seen together with low-metallicity indentations in the Galactic plane. The latter are due to foregroud/background stars in the planar bar, which in these positions dominate the bulge stars.

(ii) A metallicity gradient is present in all directions on the sky, both vertically and radially. This is expected from the binding energy argument of Sect. 3.3. However, in the central few degrees the gradients become shallower.

(iii) Iso-metallicity contours are more elongated vertically than horizontally, whereas the surface density contours are flattened to the plane (MVG11).

(iv) The asymmetry between $l > 0$ and $l < 0$ at intermediate latitudes is due to perspective effects and signifies the bar origin. In Fig. 4 high metallicities extend to larger $|l|$ on the $l > 0$ side at $|b| \simeq 5°$, but for $|b| \simeq 10°$ they extend to larger $|l|$ on the $l < 0$ side.

This map has some remarkable similarities with that being constructed from the near-infrared photometric VISTA VVV survey (Gonzalez et al. 2013). For now we can compare quantitatively with a few more measured values in off-axis fields. Details will of course depend on the parametrisation of our simple model. In the longitudinal direction the gradient along $b = 2°$ is $\alpha_l = -0.05$ dex/deg (see Fig. 2). Minniti et al. (1995) found mean metallicities [Fe/H]$= -0.3$ in two fields at $(l, b) = (8°, -7°)$ and $(10°, -7°)$ for bulge stars selected with [Fe/H]> -1. The model values in these fields are -0.30 and -0.28.

3.3. Origin of the vertical gradient

Clearly, while the bar and buckling instabilities scramble the orbits of disk stars, they do not do so enough to completely erase the preexisting metallicity gradient. High-metallicity stars tightly bound to the Galactic center initially remain more tightly bound in the final bulge, and initially more loosely bound stars with lower metallicities end up at larger final radii, on average. This can
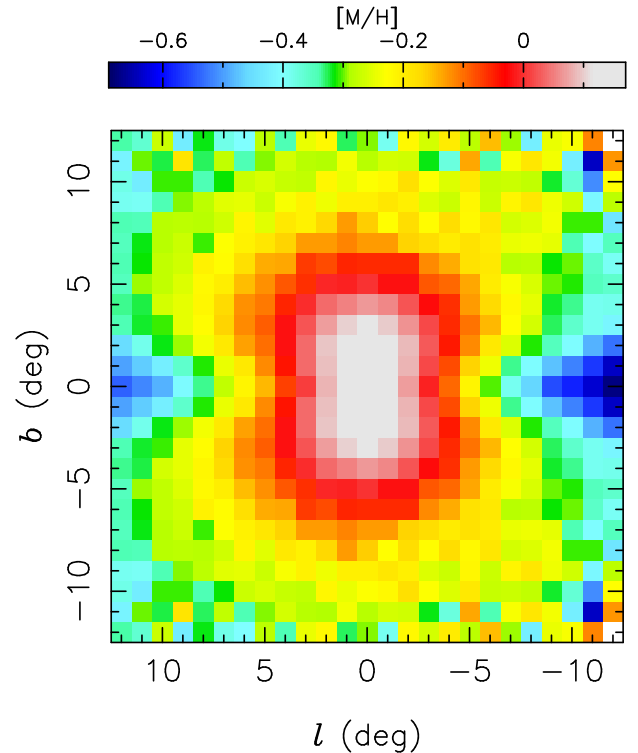

FIG. 4.— Metallicity map of the model bulge and bar in galactic coordinates. Foreground and background disk particles with distances < 4 kpc and > 12 kpc from the solar position are excluded. The colour in each square corresponds to the average metallicity in a cone with radius $0.5°$ centered at this position.

be quantified by considering the change in Jacobi energy

$$E_{\rm J} = \frac{1}{2}v^2 + \Phi(R, \phi, z) - \frac{1}{2}\Omega_p^2 R^2 \qquad (1)$$

in the rotating frame of the boxy bulge and bar during the evolution. Here we use standard cylindrical coordinates, v is total velocity, Φ is the gravitational potential, and Ω_p is the pattern speed at $T_b = 1.9$ Gyr.
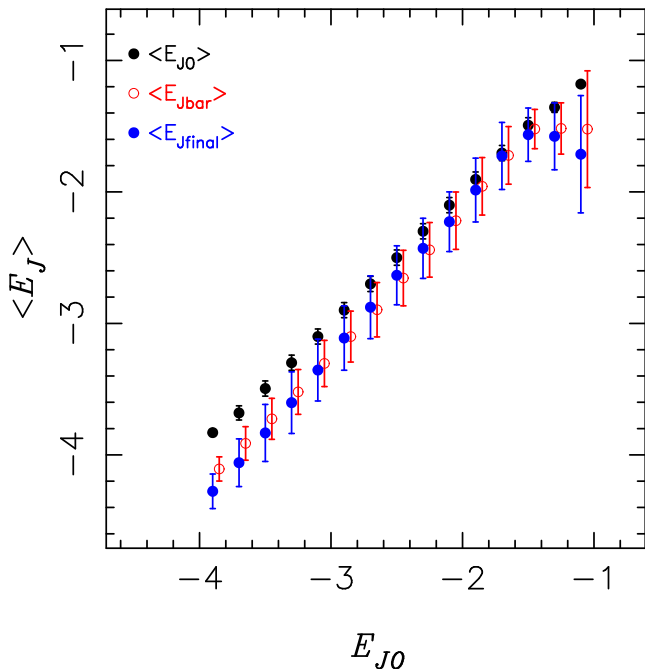
FIG. 5.— Change of Jacobi energy between different times during the evolution of the model, evaluated in a rotating frame for pattern speed $\Omega_p(T_b) = 40$ km/s/kpc. For each bin in initial Jacobi energy E_{J0}, the mean value of Jacobi energy at time t is plotted with error bars denoting the standard deviation of the distribution of $E_J(t)$ in the bin. Black points: $E_{J0}(t = 0)$ versus E_{J0} (initial scatter in each bin). Blue points: $E_{Jfinal}(t = T_b)$ versus E_{J0} (final boxy bulge compared to initial disk). Red open circles (slightly displaced horizontally for clarity): $E_{Jbar}(t = T_{bar})$ versus E_{J0} (after full bar growth but prior to buckling instability, compared to initial disk).

Fig. 5 shows that particles are scattered in Jacobi energy by the two instabilities, but only over a fraction of the available total range in E_J. I.e., they retain some memory of their initial values. It has also been shown that most bar particles inside the vertical inner Lindblad resonance (VILR) mix during the buckling instability, but stay in the inner bar regions, while most bar particles around VILR are scattered to orbits which can visit larger heights (Pfenniger & Friedli 1991; Martinez-Valpuesta & Shlosman 2004).

From these arguments follows that the number of high-metallicity particles in the final boxy bulge will decrease with height above the plane where E_J becomes less negative. In the histograms of Fig. 3, therefore, the number of stars on the metal-rich part of the distribution decreases with latitude. The maximum metallicity in all histograms, but that at $b = -12°$, is still given by the assumed maximum metallicity at the center of the initial disk, here $+0.6$, because a small fraction of the tightly bound particles is scattered up even to $b = 8°$.

The low-metallicity tail, on the other hand, is more prominent at high latitudes, because of the larger fraction of particles coming from the outer parts of the bar. Note that within the assumed model, a lower limit to the metallicity in the bulge fields is expected, which is set by the outer boundary of the part of the disk which participates in the instability. From the histograms in Fig. 3, this is $\simeq -1.2$, which is due to particles in the initial disk at $R = 4.5$kpc, just inside the corotation radius of the bar before buckling, 4.7 kpc.

These properties of the model histograms are surprisingly similar to those of the Galactic bulge MDFs discussed in the literature. If our scenario were the full explanation for the metallicity structure of the Galactic bulge, the observed range in the metallicity histograms could be used directly to estimate the central metallicity and the radial gradient in the inner Galactic disk prior to bar formation and buckling. The observational histograms, however, also contain metal-poor stellar halo and thick disk stars, and possibly metal-rich disk stars formed after the buckling, which must be taken into account in this argument. Finally we note that a radial metallicity gradient in the precursor disk could have been accompanied by a stellar age gradient. In the context of the present model, depending on the time of buckling, this could lead to a measurable vertical age gradient in the boxy bulge which would provide an independent test of the model.

3.4. Boxy bulges in other galaxies

Vertical gradients have so far been published only for a small number of galaxies with boxy bulges. Falcón-Barroso et al. (2004); Jablonka et al. (2007) found a vertical metallicity gradient in NGC 7332 comparable to that in the Milky Way. Williams et al. (2011) determined vertical gradients in two other boxy bulges, NGC 1381 and NGC 3390. They integrated along slits parallel to the major axis to increase signal-to-noise, and obtained a single bulge measurement at several z. A similar averaging over $l \in [-5°, 5°]$ in our model reduces the measured gradient from $\alpha_z = -0.46$ dex/kpc to $\alpha_z = -0.33$ dex/kpc, because radial and vertical gradients are comparable. Still, in NGC 1381 the observations show a strong gradient of averaged $\alpha_z = -0.27$ dex/kpc, while only a weak gradient is seen in NGC 3390, $\alpha_z = -0.1$ dex/kpc ($z \in [5, 10]$ arcsec). Pérez & Sánchez-Blázquez (2011) found negative metallicity gradients along the *major axis* for the majority of bulges in barred galaxies, while Williams et al. (2012) found a range of major axis metallicity gradients in boxy bulges, from negative to positive, with shallower sample average than for unbarred early-type galaxies. In summary, the limited data suggest a range of metallicity gradients in boxy bulges, with the metallicity gradient in the Milky Way on the steep side. In the framework discussed here, this suggests a range of initial disk metallicity gradients before buckling in these galaxies, perhaps depending on the time of bulge formation.

3.5. Comparison with previous simulations

The results presented in the previous subsections are consistent with early N-body simulation work by Friedli (1998). He found that pre-existing *vertical* abundance gradients in the disk were quickly flattened both in the bar and disk regions but not entirely erased. Their models also included a shallow, outward *radial* gradient, which became much flatter in the disk region due to the mixing induced by the bar, but was approximately preserved in the bar region. Friedli (1998) also stated that when no initial vertical gradient was present, a negative vertical gradient appeared at $R = 0$. However, in his model the initial gradient was $\alpha_R = -0.1$ dex/kpc, while the model analyzed here has initial $\alpha_R = -0.4$ dex/kpc,

for similar bar size. In our model the final gradient along the bar is $\alpha_R = -0.26$ dex/kpc and the final vertical gradient is $\alpha_z = -0.46$ dex/kpc (for $b \in [-3°, -7°]$). Consistent with Friedli (1998) we also find that at larger l the vertical gradient is shallower (Fig 2, *right*).

Recent N-body numerical simulations by Bekki & Tsujimoto (2011) for a pure exponential disk initial model (PDS in their nomenclature) showed only a very shallow vertical gradient in the final boxy bulge. The difference to our results can be traced to the different initial disk metallicity profile. While their inner disk parameters are similar to ours, due to linking the profile to the present metallicity near the Sun, their profile becomes quite shallow beyond $\simeq 0.25$ times the eventual final bar length. Thus the stars in the upper bulge which come from the outer parts of the bar are quite metal-rich. The difference, and the reason for the steep vertical gradient in the bulge of our model is its steep initial radial gradient in the disk.

Finally we note that if the secular evolution proceeds slowly, a radial gradient in the disk before the instability may be (partially) erased by migration processes. Thus a steep final bulge gradient is favoured by rapid secular evolution such as in the model investigated here.

4. CONCLUSIONS

We can summarize our conclusions as follows:

(i) The vertical metallicity gradient observed in the Galactic bulge can be reproduced with a secularly evolved barred galaxy model in which a boxy bulge formed after a buckling instability. In itself, a vertical gradient is therefore not a strong argument for the existence of a classical bulge in the Milky Way.

(ii) Mixing during the bar and buckling instabilities is incomplete, and therefore radial metallicity gradients in the initial disk can transform into gradients in the boxy bulge.

(iii) In this framework, the range of bulge star metallicities at various latitudes constrains the radial gradient in the precursor disk.

(iv) The full bulge metallicity map shows an overall radial gradient on the sky as well as longitudinal perspective asymmetries. Iso-metallicity contours are elongated vertically.

(v) Depending on when the bulge formed and on the properties of the precursor disk at that time, boxy bulges may or may not show metallicity gradients.

The success of our simple model in explaining Milky Way observations suggests that its underlying idea has some merit and should be pursued further. Future work also needs to consider chemical evolution and possible vertical metallicity gradients in the initial disk, star formation induced by the bar, the possible late build-up of a metal rich inner disk, and the contribution of halo stars and other components (Ness et al. 2012b) to the bulge MDFs.

Another important next step for understanding the origin of the Milky Way bulge is to investigate the correlations between metallicities and kinematics in this model and in generalisations of it. Comparison with similar observations (Babusiaux et al. 2010; Ness et al. 2012b) is likely to shed light on the possible multi-component nature of the Galactic bulge. The results will be important also for interpreting the data for bulges in external galaxies.

REFERENCES

Athanassoula, E., & Misiriotis, A. 2002, MNRAS, 330, 35
Babusiaux, C., Gómez, A., Hill, V., et al. 2010, A&A, 519, A77
Bekki, K., & Tsujimoto, T. 2011, MNRAS, 416, L60
Benjamin, R. A., Churchwell, E., Babler, B. L., et al. 2005, ApJ, 630, L149
Binney, J., Gerhard, O., & Spergel, D. 1997, MNRAS, 288, 365
Bureau, M., & Athanassoula, E. 2005, ApJ, 626, 159
Bureau, M., & Freeman, K. C. 1999, AJ, 118, 126
Cabrera-Lavers, A., Hammersley, P. L., González-Fernández, C., et al. 2007, A&A, 465, 825
Clarkson, W., Sahu, K., Anderson, J., et al. 2008, ApJ, 684, 1110
Combes, F., Debbasch, F., Friedli, D., & Pfenniger, D. 1990, A&A, 233, 82
Debattista, V. P., Carollo, C. M., Mayer, L., & Moore, B. 2004, ApJ, 604, L93
Dwek, E., Arendt, R. G., Hauser, M. G., et al. 1995, ApJ, 445, 716
Falcón-Barroso, J., Peletier, R. F., Emsellem, E., et al. 2004, MNRAS, 350, 35
Friedli, D. 1998, in Astronomical Society of the Pacific Conference Series, Vol. 147, Abundance Profiles: Diagnostic Tools for Galaxy History, ed. D. Friedli, M. Edmunds, C. Robert, & L. Drissen, 287
Friedli, D., Benz, W., & Kennicutt, R. 1994, ApJ, 430, L105
Gerhard, O., & Martinez-Valpuesta, I. 2012, ApJ, 744, L8
Gonzalez, O. A., Rejkuba, M., Zoccali, M., et al. 2013, arXiv:1302.0243
Gonzalez, O. A., Rejkuba, M., Zoccali, M., et al. 2012, A&A, 543, A13
—. 2011, A&A, 530, A54
Howard, C. D., Rich, R. M., Clarkson, W., et al. 2009, ApJ, 702, L153

Ibata, R. A., & Gilmore, G. F. 1995, MNRAS, 275, 591
Jablonka, P., Gorgas, J., & Goudfrooij, P. 2007, A&A, 474, 763
Johnson, C. I., Rich, R. M., Fulbright, J. P., Valenti, E., & McWilliam, A. 2011, ApJ, 732, 108
Li, Z.-Y., & Shen, J. 2012, ApJ, 757, L7
López-Corredoira, M., Cabrera-Lavers, A., & Gerhard, O. E. 2005, A&A, 439, 107
Lütticke, R., Dettmar, R.-J., & Pohlen, M. 2000, A&AS, 145, 405
Martinez-Valpuesta, I., & Gerhard, O. 2011, ApJ, 734, L20
Martinez-Valpuesta, I., & Shlosman, I. 2004, ApJ, 613, L29
Martinez-Valpuesta, I., Shlosman, I., & Heller, C. 2006, ApJ, 637, 214
McWilliam, A., & Zoccali, M. 2010, ApJ, 724, 1491
Minniti, D., Olszewski, E. W., Liebert, J., et al. 1995, MNRAS, 277, 1293
Nataf, D. M., Udalski, A., Gould, A., Fouqué, P., & Stanek, K. Z. 2010, ApJ, 721, L28
Ness, M., Freeman, K., Athanassoula, E., et al. 2012a, ApJ, 756, 22
Ness, M., Freeman, K., Athanassoula, E., et al. 2012b, arXiv preprints
Pérez, I., & Sánchez-Blázquez, P. 2011, A&A, 529, A64
Pfenniger, D., & Friedli, D. 1991, A&A, 252, 75
Rich, R. M. 1990, ApJ, 362, 604
Rich, R. M., Origlia, L., & Valenti, E. 2007, ApJ, 665, L119
—. 2012, ApJ, 746, 59
Shen, J., Rich, R. M., Kormendy, J., et al. 2010, ApJ, 720, L72
Skrutskie, M. F., Cutri, R. M., Stiening, R., et al. 2006, AJ, 131, 1163
Williams, M. J., Bureau, M., & Kuntschner, H. 2012, MNRAS, L537

Williams, M. J., Zamojski, M. A., Bureau, M., et al. 2011, MNRAS, 414, 2163

Zoccali, M., Hill, V., Lecureur, A., et al. 2008, A&A, 486, 177

Zoccali, M., Renzini, A., Ortolani, S., et al. 2003, A&A, 399, 931